Nanoscale Res Lett (2009) 4:753–757
DOI 10.1007/s11671-009-9310-1

NANO EXPRESS

Mechanical Deformation Behavior of Nonpolar GaN Thick Films by Berkovich Nanoindentation

Tongbo Wei · Qiang Hu · Ruifei Duan · Junxi Wang · Yiping Zeng · Jinmin Li · Yang Yang · Yulong Liu

Received: 2 February 2009 / Accepted: 2 April 2009 / Published online: 25 April 2009

Abstract In this study, the deformation mechanisms of nonpolar GaN thick films grown on m-sapphire by hydride vapor phase epitaxy (HVPE) are investigated using nanoindentation with a Berkovich indenter, cathodoluminescence (CL), and Raman microscopy. Results show that nonpolar GaN is more susceptible to plastic deformation and has lower hardness than *c*-plane GaN. After indentation, lateral cracks emerge on the nonpolar GaN surface and preferentially propagate parallel to the $\langle 11\bar{2}0 \rangle$ orientation due to anisotropic defect-related stresses. Moreover, the quenching of CL luminescence can be observed to extend exclusively out from the center of the indentations along the $\langle 11\bar{2}0 \rangle$ orientation, a trend which is consistent with the evolution of cracks. The recrystallization process happens in the indented regions for the load of 500 mN. Raman area mapping indicates that the distribution of strain field coincides well with the profile of defect-expanded dark regions, while the enhanced compressive stress mainly concentrates in the facets of the indentation.

Keywords GaN · Nonpolar · HVPE · Nanoindentation · Cathodoluminescence · Raman mapping

T. Wei (✉) · Q. Hu · R. Duan · J. Wang · Y. Zeng · J. Li
Semiconductor Lighting Technology Research and Development Center, Institute of Semiconductors, Chinese Academy of Sciences, Beijing 100083, People's Republic of China
e-mail: tbwei@semi.ac.cn

Y. Yang · Y. Liu
Institute of Physics, Chinese Academy of Sciences, Beijing 100190, People's Republic of China

Introduction

GaN-related III-nitride materials have drawn much attention over the last decade owing to its highly expected potential in short-wavelength optoelectronic devices, optical detectors, and semiconductor lasers [1, 2]. In order to further improve the performance of these devices, besides the optical and electrical properties of materials, mechanical characteristics and deformation behavior are also crucial for solving the problems of residual stress/strain introduced by heteroepitaxial films and multiple-layer device structures. Furthermore, semiconductor device processing involves extensively with surface contact, cracking, film delamination, and propagation of dislocations, which may degrade the performance of these devices. Consequently, significant interest in determining the mechanical characterizations of GaN materials is motivated, in particular at the nanoscale level, both in basic research and technological applications.

In this respect, nanoindentation has proven to be a powerful technique for probing the information on the mechanical properties of GaN thin films and substrates with characteristic dimensions in the sub-micron regime, such as hardness and elastic modulus, creep resistance, fracture toughness, and adhesion [3–6]. The load–displacement curves also reveal the various structural changes within the indented materials during nanoindentation [7, 8]. However, most of the nanoindentation studies were carried out on *c*-plane GaN films or bulk single crystals at present. To our knowledge, there are only few reports available on the mechanical deformation behavior of nonpolar GaN epitaxial layers, which have been receiving considerable attention to alleviate the spontaneous and strain-induced piezoelectric polarization effects. Such knowledge is of great importance for realizing better manufacturing

processes and device stability of nonpolar GaN. In this study, we investigate the main deformation features of nonpolar *m*-plane GaN thick films during nanoindentation. Moreover, we also discuss how these features correlate with indentation-produced defect microstructures revealed by Raman scattering and cathodoluminescence (CL) microscopy.

Experimental Details

The undoped wurtzite *m*-plane and *c*-plane GaN epilayers with a thickness of nearly 50 μm, grown by hydride vapor phase epitaxy (HVPE) method, was used in this study. The detailed growth procedures and structural characterization of the GaN epitaxial layers could be found elsewhere [9]. The nanoindentation tests were performed on MTS Nano Indenter XP system with a continuous contact stiffness measurement (CSM) technique. A diamond pyramid-shaped Berkovich-type indenter tip, whose radius of curvature is approximately 50 nm, was employed for the indentation experiments. All necessary experimental parameters, such as the tip area function and frame compliance, were calibrated prior to each set of experiments using a standard fused silica specimen. A series of continuous load–unload indents were carried out at the load range of 5–500 mN. At least five independent measurements were made for one experimental point. Each indentation was separated by 50 μm to avoid possible interferences between neighboring indents. Here, all indents were performed at room temperature. The analytic method developed by Oliver and Pharr was adopted to determine the hardness (H) and Young's modulus (E) of GaN films from the load–displacement curves [10].

After indentation, the contact-induced defect microstructures were analyzed using CL and Raman scattering. The CL observation was performed using a Gatan MonoCL3 plus equipment, installed on a scanning electron microscope (SEM) (FEI Quanta 200FEG) at room temperature. Finally, a LabRam HR800 spectrometer with an automatized XY table of acquisition was used to record the Raman spectra with excitation wavelength of 532 nm of Ar^+ laser. Raman area mapping was also recorded for the indentation. The laser beam was focused on the sample with a spot diameter of about 1 μm and the spectral resolution was better than 0.1 cm^{-1}. All the Raman spectra were obtained in backscattering geometry.

Results and Discussion

Typical loading–unloading force–displacement curves of different crystalline plane GaN thick films are shown in Fig. 1. Similar to many previous reports [11–14], the figure illustrates a slight discontinuity ("pop-in") of the yield response for *c*-plane epilayer, which has been most commonly associated with the sudden nucleation of dislocations and propagation along easy slip systems. However, for an *m*-plane film, much larger pop-in discontinuity occurs. The longer pop-in length illustrates that the nonpolar GaN surfaces are capable of accommodating more strain than *c*-plane before dislocation motion is arrested by the opposing backstress created by dislocation pile-up [15]. The origin of this discrepancy may be due to different activation of various slip systems and the surface stacking faults concomitantly within the film along nonpolar growth. Furthermore, close examination of partial load–unload curves reveals that in nonpolar GaN, there is deeper penetration and lower elastic recovery than in *c*-plane GaN at the same applied load. This result demonstrates that the nonpolar *m*-plane GaN is more susceptible to plastic deformation and has lower hardness in comparison with *c*-plane GaN. It is thus reasonable to conclude that slip and the orientation of the basal planes play a key role in defining the mechanical properties of crystalline materials.

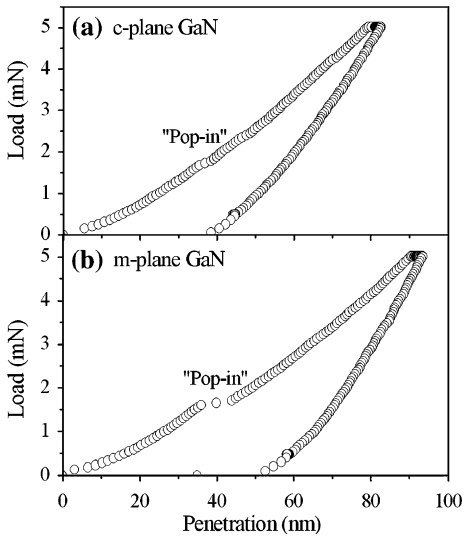

Fig. 1 Typical continuous load–unload curves of **a** c-plane and **b** m-plane nonpolar GaN thick films grown by HVPE

With the continuous contact stiffness measurements, the penetration depth dependence of the hardness and Young's modulus can be obtained, as shown in Fig. 2a and b. It is noted that the hardness of *m*-plane GaN decreases abruptly at the depth of 33 nm corresponding to the longer "pop-in" and then maintains almost constant. *c*-plane GaN epilayer is obviously harder about 2 GPa than *m*-plane GaN. The comparative softness of the *m*-plane GaN is due to the orientation of the nonpolar basal plane, and the ease in which slip can occur along the direction. On the other hand, Young's modulus E value of the *m*-plane GaN is not

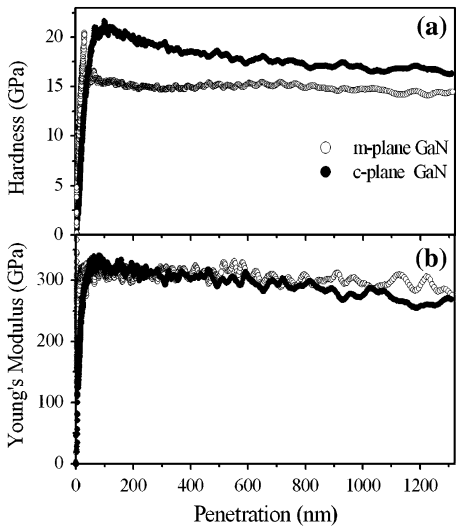

Fig. 2 The curves of **a** the hardness and **b** Young's modulus with respect to indentation depth for c-plane and m-plane GaN thick films using continuous stiffness module (CSM)

affected at all by the pop-in event and focuses on 300 GPa with small oscillations. Furthermore, the values of E for two GaN epilayers are independent of slip and the crystal orientation, which are nearly identical and remain relatively constant for the whole indenter penetration depth. This is not surprising since during indentation averaging over the stiffness' in all directions occurs. For example, even for highly anisotropic (cubic) crystals, the Young's modulus depends only slightly on the orientation of the indented plane [16].

It has previously been reported that there are no cracks formed for loads up to as high as 900 mN with spherical indenter for *c*-plane hexagonal GaN [17]. Note that for this study, three classical radial cracks emanate from the three corners of the triangular indentation at a maximum load of 500 mN for *c*-plane GaN epilayer. However, the impressions left on the *m*-plane nonpolar GaN are significantly different, and lateral cracks run through the center of the indentation irrespective of the side directions of triangular indentations, as shown in Fig. 3a and c. It is worth noting that all cracks preferentially propagate parallel to the $\langle 11\bar{2}0 \rangle$ orientation, keeping accordance with aligned directions of surface slate-like characteristic. Furthermore, slip lines can be clearly resolved in the indentation regions from both Fig. 3c and f, which act as a result of dislocations glide in the {0001} plane. At the slip-plane crossing, these defect-related stresses are expected to increase drastically due to dislocation pile-ups [18], and consequently, cracks could be preferably nucleated along the $\langle 11\bar{2}0 \rangle$ direction. It is thus evidenced that slip is the major mode of plastic deformation in nonpolar *m*-plane GaN. Another plausible candidate for aligned crack propagation is surface slates relating with the basal plane stacking faults, and the easy accumulation of the indentation-induced dislocations at the borders of the slates. In this way, the borders become sources of microcrack initiation [19].

Figure 3 also shows corresponding CL images of the *m*-plane indented regions at the load of 500 mN. These CL images clearly illustrate the distribution of deformation-induced extended defects which act as efficient nonradiative recombination centers and dramatically suppress CL emission. The quenching of luminescence can be observed to extend exclusively out from the center of the indentations along the $\langle 11\bar{2}0 \rangle$ orientation, a trend which is consistent with the evolution of cracks as discussed above. Additionally, in the perpendicular and parallel cases toward the surface slates, dark expanded regions obviously differ,

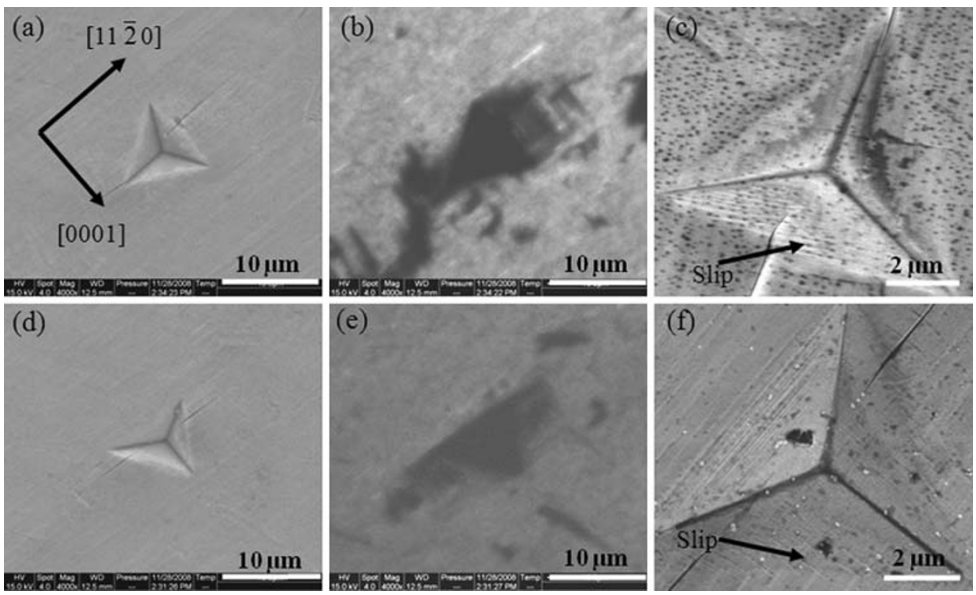

Fig. 3 SEM images of indented regions with the side perpendicular to the surface slates (**a**) and parallel to the slates (**d**) obtained at load of 500 mN on nonpolar GaN. **b** and **e** are the corresponding panchromatic CL images of (**a**) and (**d**), respectively. **c** and **f** are magnified SEM images in the perpendicular and parallel cases at 500 mN

as shown in Fig. 3b and e. This is comprehensible since the different distributions of stress near the indentations are produced at the two modes. In contrast, Jian et al. found an indentation pattern called "rosette" by CL emission, with a sixfold structure symmetry reflecting the hexagonal symmetry of *c*-plane GaN film subjected to Berkovich nanoindentation [20]. The origin of this discrepancy can be ascribed to in-plane anisotropic defects propagation on the nonpolar *m*-plane GaN surface.

Subsequently, Raman measurement is also carried out to investigate the structural transformation of the *m*-plane GaN close to the indented regions, as indicated in Fig. 4. It is interesting to note that from the matrix to the indentation center, the E2 (high) peak first shifts up to a high wavenumber and redshifts, indicating the enhanced compressive stress of the indented area. Compared to the matrix, the E2 phonon lines in the indentation are clearly broadened and display a shoulder peak at 571 cm^{-1}, confirming a poor hexagonal crystalline order after deformation [21]. Besides the double peaks, a broad A1 (LO) peak also emerges as the forbidden phonon mode. Therefore, it is deduced that the recrystallization of GaN happens due to high shear stress during the indentation process, which results in small misorientations of crystallites in the indented regions. However, no new phonon modes are observed in Fig. 4a, meaning that no pressure-induced phase transformation in the material has occurred. Somewhat similar recrystallization behavior of indented GaN was reported by Dhara et al. [22]. Nevertheless, their Raman results showed that the indentation region is stress free due to the dislocation motion compared with our compressive stress. Combining these above results, we speculate that the difference may be owing to the fact that there is no substrate influence for *m*-plane GaN thick film even at extremely high load, in contrast with 6 μm GaN epilayer in their report.

Figure 4b shows a map of the E2 (high) phonon frequency from the region of the indentation in Fig. 3a. In the indentation regions, it is apparent that the enhanced compressive stress mainly concentrates in the facets. The stress at the center is partly released due to the heavily deformed and strain-hardened lattice structure, suffered from the highest pressure under the indenter tip. Therefore, the high defect structure leads to the Raman shift shown in green at the indentation center. Outside the indentation, the formation of cracks does not cause the local stress relaxation as expected and instead leads to the increase of stress. Furthermore, a comparison of CL and Raman mapping clearly illustrates that the size of the dark defect-expanded regions observed in CL images around indentation coincides well with the profile of red regions with high compressive stress. However, in the defect-expanded regions outside the imprint, the E2 (high) mode remains still

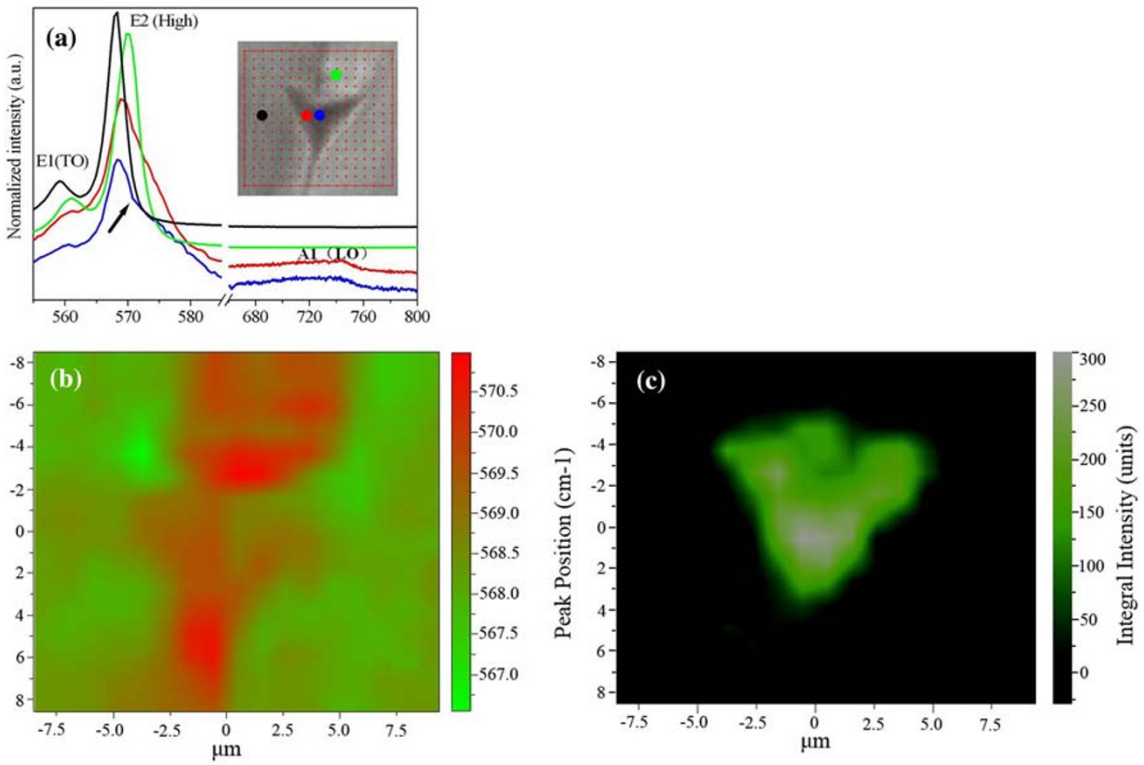

Fig. 4 **a** Micro-Raman spectra acquired from different spots at load of 500 mN on m-plane GaN. **b** Frequency map of the E2 mode, and **c** Spatial distribution of the integral intensity of A1(LO) peak in the indented regions

symmetric and slightly broadened, and no A1 (LO) mode can be observed as shown in Fig. 4c. It is thus deduced that the recrystallization process does not happen in the defect-expanded regions despite the high residual stress.

Conclusions

In order to summarize, details of nanoindentation-induced mechanical deformation of nonpolar *m*-plane GaN thick films fabricated by HVPE method have been studied by nanoindentation in combination with CL and Raman. In comparison with *c*-plane GaN, nonpolar GaN has the longer pop-in length and lower hardness, confirming that the orientation of the basal planes plays a key role in defining the mechanical properties of hexagonal GaN. Indentation at high load can produce slip lines and lateral cracks, preferentially propagating along the $\langle 11\bar{2}0 \rangle$ orientation. The comparison of CL and Raman mapping clearly illustrates that defect-expanded regions observed in CL images are in agreement with the profile of regions with high compressive stress, which represents anisotropic pattern. Finally, the recrystallization behavior is observed in the indented regions of nonpolar GaN at a maximum load up to 500 mN.

Acknowledgments This study was supported by the National High Technology Program of China under Grant No. 2006AA03A143, the National Natural Sciences Foundation of China under Grant No. 60806001, and the Knowledge Innovation Program of the Chinese Academy of Sciences under Grant No. ISCAS2008T03. We would also like to thank Professor Li Chen of Peking University for his assistance in the Cathodoluminescence experiments.

References

1. S. Nakamura, M. Senoh, S. Nagahama, N. Iwasa, T. Yamada, T. Matsushita, H. Kiyoku, Y. Sugimoto, Appl. Phys. Lett. **68**, 2105 (1996). doi:10.1063/1.115599
2. G. Fasol, Science **272**, 1751 (1996). doi:10.1126/science.272.5269.1751
3. R. Nowak, M. Pessa, M. Suganuma, M.I. Leszczynski, S. Grzegory, S. Porowski, F. Yoshida, Appl. Phys. Lett. **75**, 2070 (1999). doi:10.1063/1.124919
4. S. Basu, M.W. Barsoum, A.D. Williams, T.D. Moustakas, J. Appl. Phys. **101**, 083522 (2007). doi:10.1063/1.2719016
5. S.O. Kucheyev, J.E. Bradby, J.S. Williams, C. Jagadish, M.V. Swain, G. Li, Appl. Phys. Lett. **78**, 156 (2001). doi:10.1063/1.1335552
6. R. Navamathavan, Y.T. Moon, G.S. Kim, T.G. Lee, J.H. Hahn, S.J. Park, Mater. Chem. Phys. **99**, 410 (2006). doi:10.1016/j.matchemphys.2005.11.021
7. S.R. Jian, Nanoscale Res. Lett. **3**, 6 (2008). doi:10.1007/s11671-007-9106-0
8. J.E. Bradby, J.S. Williams, M.V. Swain, J. Mater. Res. **19**, 380 (2004). doi:10.1557/jmr.2004.19.1.380
9. T.B. Wei, R.F. Duan, J.X. Wang, J.M. Li, Z.Q. Huo, J.K. Yang, Y.P. Zeng, Jpn. J. Appl. Phys. **47**, 3346 (2008). doi:10.1143/JJAP.47.3346
10. W.C. Oliver, G.M. Pharr, J. Mater. Res. **7**, 1564 (1992). doi:10.1557/JMR.1992.1564
11. J.E. Bradby, S.O. Kucheyev, J.S. Williams, J.W. Leung, M.V. Swain, P. Munroe, G. Li, M.R. Phillips, Appl. Phys. Lett. **80**, 383 (2002). doi:10.1063/1.1436280
12. D. Caceres, I. Vergara, R. Gonzalez, E. Monroy, F. Calle, E. Munoz, F. Omnes, J. Appl. Phys. **86**, 6773 (1999). doi:10.1063/1.371726
13. G. Yu, H. Ishikawa, T. Egawa, T. Soga, J. Watanabe, T. Jimbo, M. Umeno, J. Cryst. Growth **189/190**, 701 (1998). doi:10.1016/S0022-0248(98)00262-0
14. V.A. Coleman, J.E. Bradby, C. Jagadish, P. Munroe, Y.W. Heo, S.J. Pearton, D.P. Norton, M. Inoue, M. Yano, Appl. Phys. Lett. **86**, 203105 (2005). doi:10.1063/1.1929874
15. W.W. Gerberich, J.C. Nelson, E.T. Lilleodden, P. Anderson, J.T. Wyrobek, Acta Mater. **9**, 3585 (1996). doi:10.1016/1359-6454(96)00010-9
16. W.D. Nix, Mater. Sci. Eng. A **234**, 37 (1997). doi:10.1016/S0921-5093(97)00176-7
17. S.O. Kucheyev, J.E. Bradby, J.S. Williams, C. Jegadish, M. Toth, M.R. Phillips, M.V. Swain, Appl. Phys. Lett. **77**, 3373 (2000). doi:10.1063/1.1328047
18. U. Jahn, A. Trampert, T. Wagner, O. Brandt, K.H. Ploog, Phys. Status. Solidi. **192**, 79 (2002). doi:10.1002/1521-396X(200207)192:1<79::AID-PSSA79>3.0.CO;2-5
19. P. Kavouras, P. Komninou, M. Katsikini, V. Papaioannou, J. Antonopoulos, T. Karakostas, J. Phys. Condens. Matter. **12**, 10241 (2000). doi:10.1088/0953-8984/12/49/324
20. S.R. Jian, I.J. Teng, J.M. Lu, Nanoscale Res. Lett. **3**, 158 (2008). doi:10.1007/s11671-008-9130-8
21. P. Puech, F. Demangeot, J. Frandon, C. Pinquier, M. Kuball, V. Domnich, Y. Gogotsi, J. Appl. Phys. **96**, 2853 (2004). doi:10.1063/1.1775295
22. S. Dhara, C.R. Das, H.C. Hsu, B. Raj, A.K. Bhaduri, L.C. Chen, K.H. Chen, S.K. Albert, A. Ray, Appl. Phys. Lett. **92**, 143114 (2008). doi:10.1063/1.2907851